Microdroplet fabrication of silver–agarose nanocomposite beads for SERS optical accumulation†‡

Sara Abalde-Cela,[a] Baptiste Auguié,[a] Martin Fischlechner,[b] Wilhelm T. S. Huck,[b] Ramón A. Alvarez-Puebla,*[a] Luis M. Liz-Marzán*[a] and Chris Abell*[b]

Microdroplets have been used as reactors for the fabrication of agarose beads with high uniformity in shape and size, and densely loaded with silver ions, which were subsequently reduced into nanoparticles using hydrazine. The resulting nanocomposite beads not only display a high plasmonic activity, but can also trap/concentrate analytes, which can be identified by means of surface-enhanced Raman scattering (SERS) spectroscopy. The size of the beads is such that it allows the detection of a single bead under a conventional optical microscope, which is very useful to reduce the amount of material required for SERS detection.

Introduction

Surface-enhanced Raman scattering (SERS) spectroscopy has evolved as a powerful and ultrasensitive tool for the detection and identification of a wide range of relevant analytes[1,2] down to the limit of single molecule detection.[3–5] As a result, a new family of plasmonic materials has emerged to solve the inherent drawbacks of metal colloids, such as limited stability[6] or the difficulty of generating efficient hot spots.[7,8] These novel materials comprise an assembly of metallic nanoparticles adsorbed on the surface of a bigger particle (which can range from nm to mm), usually made of a polymer, an inorganic oxide such as silica or titania,[9,10] or even carbon nanotubes.[11] Coating approaches include *in situ* reduction of metal ions on the surface of the support[12,13] or *ex situ* adsorption of preformed colloids using layer-by-layer[11,14] or self-assembly[10,15] for functionalization of the supporting platform, or even subjecting the support to a swelling–deswelling process in the presence of nanoparticles.[16,17] These composite particles work as optically stable, discrete surfaces, as opposed to extended media such as colloidal suspensions or massive nanoparticle thin films. Furthermore, when the beads are large enough to be localized under an optical microscope, one single particle can be enough to carry out SERS analysis. This dramatically increases the detection limits of the technique, as much less analyte is required to generate an adequate SERS signal.[14] Unfortunately, most of the methods currently available to produce the supporting materials, such as mini-, micro-, emulsion or suspension polymerization, yield particles that are either inconveniently small or heterogeneous in size. This increases the price of the materials significantly because

several purification steps are required to narrow the size distribution of the particles. Moreover, the low affinity of a wide range of analytes for gold or silver surfaces,[18] the most common and efficient SERS substrates,[19] persists within these composite materials.

Recently, a new concept of molecular trapping and concentration based on mechanical forces promoted by low SERS cross-section, stimuli responsive polymers[18,20,21] rather than electrostatic,[22] hydrophobic[23–25] or specific[11,26] host–guest interactions has emerged as an alternative for the ultrasensitive detection of a wide range of molecular species. These trapping substrates have been presented in different formats, from single particles through thin films to macroscopic three dimensional gels. However, the development of discrete and homogeneous composite particles containing a high density of hot spots is still required.

Microfluidic technology is an emerging application area characterized by the controlled handling of nano- and picolitre volumes into microchannels. Microfluidic systems can be applied in a variety of fields ranging from molecular biology, clinical pathology or controlled fabrication of materials. Recently, there has been a tremendous interest in the use of microdroplets in microfluidics (also called 'biphasic', 'segment' or 'plug-based' microfluidics) for chemical and biological reactions in controlled environments.[27] In essence, each droplet is analogous to the traditional chemist's flask, with the added physical advantages of reduced reagent consumption, rapid mixing, automated handling, and continuous rather than batch processing. The monodisperse nature of microdroplets produced in microfluidic channels can provide a unique reaction environment for the formation of highly uniform particles, gel beads and capsules.[28] Agarose gel particles can be formed by simply cooling liquid droplets after their formation.[29] Several reports have also demonstrated the formation of particles composed of alginate,[30] where gelation is dependent on divalent cations as crosslinking agents and occurs at very high rate. Premature gel formation can be avoided by separating laminar co-flowing Na–alginate and $CaCl_2$ solutions with a water stream before droplet formation; when the contents are mixed inside the droplets, gelation occurs very rapidly.[31] This ability to combine different aqueous flows

[a]*Departamento de Química Física and Unidad Asociada CSIC-Universidade de Vigo, 36310 Vigo, Spain. E-mail: ramon.alvarez@uvigo.es; lmarzan@uvigo.es; Fax: +34 9868 12556; Tel: +34 9868 12298*
[b]*Department of Chemistry, Lensfield Road, Cambridge, CB2 1EW, UK. E-mail: ca26@cam.ac.uk; Fax: +44 (0)1223 336362; Tel: +44 (0)1223 336405*

into droplets also offers an opportunity to load the gel particles formed with different components. These characteristics can be exploited for the production of discrete, highly active composite plasmonic platforms on demand.

Here we present a new method based on microdroplet technology, for the fabrication of composite (polymer–silver nanoparticle) beads that are homogeneous in shape and size. This material encompasses a combination of colloidal stability, the ability to trap/concentrate analytes, and an adequate size that allows the detection of a single bead under a conventional optical microscope (thereby requiring a very small amount of material for SERS detection), with a high plasmonic activity. Altogether, these beads allow for ultrasensitive determination of analytes in solution down to the femtomolar regime.

Results and discussion

Microfluidic PDMS/glass devices were fabricated by conventional soft lithography methods,[32] using different designs (one or two aqueous inlets) so as to identify the optimum configuration that would allow the fabrication of the desired nanocomposite material. A first approach toward metal particle loaded agarose beads was based on direct encapsulation of preformed colloidal nanoparticles, using gold colloids containing either nanostars or nanospheres,[33] by means of a chip with one aqueous inlet similar to that described in Fig. 1. This method however, yielded materials with low nanoparticle loadings due to the intrinsic instability of highly concentrated nanoparticle colloids. Although loading can be significantly increased by stabilizing the nanoparticles with capping agents such as polyvinylpyrrolidone (PVP) or cetyltrimethylammonium bromide (CTAB),[34] which prevent aggregation thereby giving rise to highly concentrated
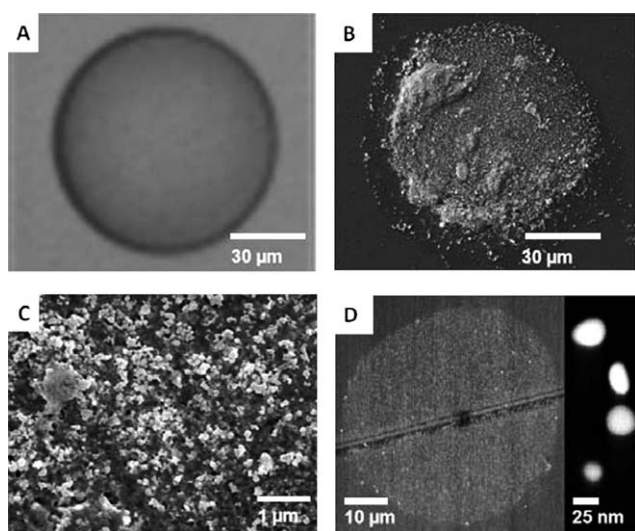
nanoparticle dispersions, this approach is not appropriate for SERS because it dramatically hinders the interaction between the analyte and the nanostructured metal surface. Consequently the preparation of the composite materials was carried out using a device with two aqueous inlets (Fig. S1†). Briefly, this approach is based on the introduction of an aqueous flow containing agarose and metal ions. This flow converges with a second stream containing a solution of either sodium borohydride or ascorbic acid, which act as reducing agents, immediately prior to the flow focusing junction where microdroplet formation occurs in the organic phase (fluorous oil containing surfactant). One drawback found with this method was the generation of hydrogen in the channels, which perturbed droplet formation (Fig. S2†). This bubble formation can be avoided by changing the reducing agent to hydrazine. Notwithstanding, the SERS efficiency of these composites was still low due to either the loss of metal because of the formation of a silver coating on the channel walls (see Movie S1†) or the formation of large, micron-sized silver particles (see Fig. S3†) on the surface of the agarose beads. Thus, instead of fabricating the agarose–nanoparticle composites entirely in emulsion, agarose with metal ions was emulsified and the hydrogel gelled by cooling. After breaking the emulsion, the metal ions inside the gel beads were reduced into nanoparticles by simply adding hydrazine to the dispersion. Fig. 1 shows a detailed scheme and optical images of the two inlet microdroplet device. In this device, an aqueous flow containing agarose and silver nitrate (inlet A) was injected through the flow-focusing system into the oil phase comprising the fluorous oil and surfactant (inlet B), forming homogenous droplets with diameters around 75 μm (see Movie S2†). The experiment was carried out above 30 °C to avoid early gelation of the agarose solution. The droplets were then collected in a plastic tube on ice to
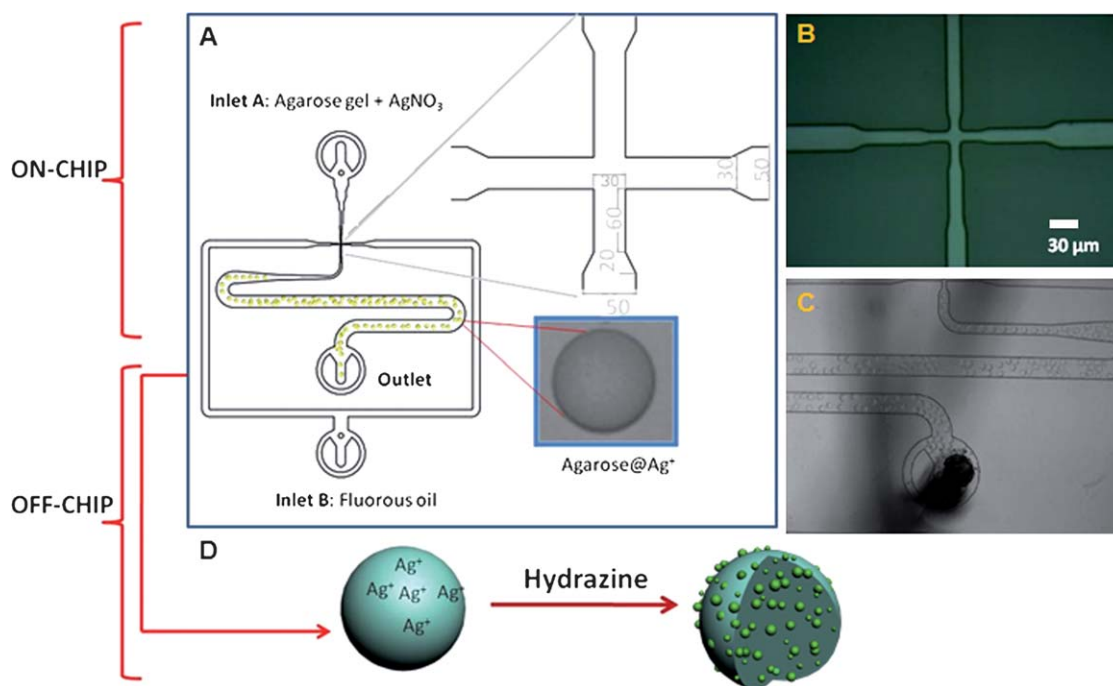

Fig. 1 (A) Detailed scheme for the on-chip preparation of homogenous Ag+–agarose microbeads (inset). Optical images of the T-junction and flow-focusing system (B), and the chip channels and outlet containing the prepared microbeads (C). (D) Off-chip reduction of the silver ions into nanoparticles inside the beads.

promote gelation of the agarose beads, and extracted into an aqueous phase using 1H,1H,2H,2H-perfluoro-1-octanol. Hydrazine was then added to reduce the Ag+, resulting in a sudden change of the initially colourless beads into a dark green colour, indicating the formation of AgNPs inside the agarose gel, as confirmed in Fig. 1D. Reduction could also be achieved using sodium borohydride, but no SERS signal could be obtained in this case because silver nanoparticles leached out from the beads during the cleaning process.

Optical (Fig. 2A and S4†) and SEM (Fig. 2B–D) characterization confirmed the formation of homogeneous agarose beads with diameters around 75 μm. Notably, no significant changes in diameter were measured upon bead dehydration (Fig. 2B), whereas their height decreased from 75 down to ∼10 μm, probably because the gel collapsed on the support. This indicates a reduction in the volume of the beads of around tenfold upon dehydration, which is consistent with what has been reported for similar materials.[20] Detailed SEM imaging of the surfaces and cross-sections of the beads (Fig. 2C, D and S5†) shows that not only is the surface completely coated with silver particles, ranging from 30 to 50 nm, but they are also formed in the interior of the beads. Remarkably, localized surface plasmon resonance (LSPR) scattering bands (Fig. 3A) for these materials, obtained by imaging the same bead before and after dehydration under a dark field optical microscope coupled to a spectroscopic CCD camera (see Experimental), display a maximum around 700 nm that hardly red-shifts after drying. Considering that non-interacting silver nanoparticles of similar dimensions present an LSPR maximum around 420 nm and that the effect of the medium refractive index usually does not lead to plasmon red-shifts above few tens of nanometres,[35] the observed shift is presumably due to the dense formation of nanoparticle aggregates, giving rise to plasmon coupling. This idea is consistent with the semi-quantitative analysis obtained with XPS (Fig. S6†) that indicates 14.8 atomic% of silver on the beads as prepared, and 34.9% after an Ar ion sputtering treatment, which removes
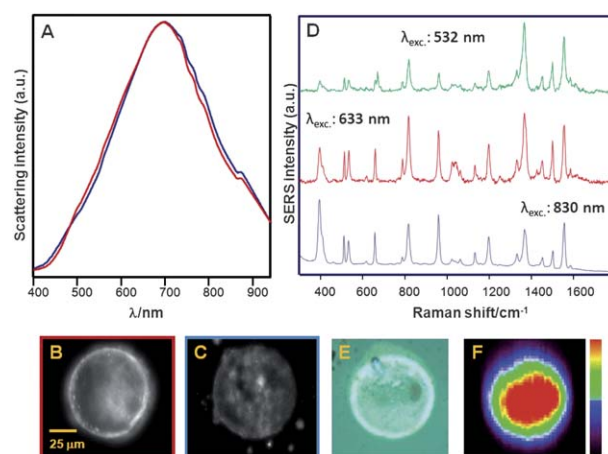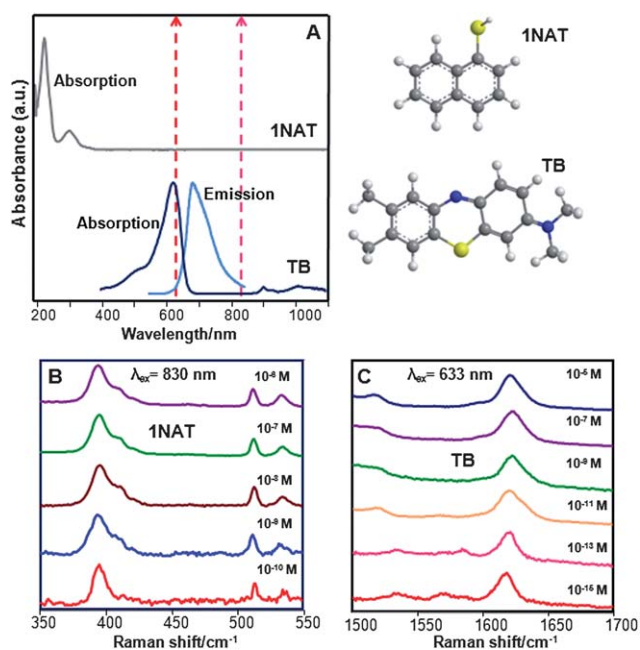

Fig. 3 (A) Localized surface plasmon resonance bands of the Ag–agarose beads before (red) and after (blue) dehydration. Dark field images of the same bead before (B) and after (C) dehydration. (D) SERS spectra of 1NAT acquired on the beads using different excitation laser lines. (E and F) Optical and SERS mapping images of 1NAT (1553 cm⁻¹) on the bead (λ_{ex} = 633 nm, 100 × 100 μm², step size 2 μm; 2500 spectra).

the organic materials, showing the high concentration of silver inside the bead.

The SERS efficiency of the beads was tested with several excitation laser lines, by adding 1-naphthalenethiol (1NAT) to a dilute bead suspension, and letting it chemisorb on the silver nanoparticles. A small volume containing several beads was then cast and air-dried onto a glass slide. In all cases, extremely strong SERS signals were acquired for the 1NAT characteristic bands (Fig. 3D): ring stretching (1553, 1503, and 1368 cm⁻¹), CH bending (1197 cm⁻¹), ring breathing (968 and 822 cm⁻¹), ring deformation (792, 664, 539, and 517 cm⁻¹), and CS stretching (389 cm⁻¹), even when using a very low laser power at the sample (∼1 μW with acquisition times of 10 s). SERS mapping of a silver-loaded bead was carried out using the 830 nm laser line (Fig. 3E and F). The results clearly indicate that Ag–agarose bead films render an exceptionally efficient, portable SERS platform for a wide range of excitation laser lines, with high and homogeneous signal intensity over the entire surface, which is often a critical parameter when dealing with hot spots built on solid thin supports. Further, this also indicates the formation of a large number of highly active hot spots on and inside the polymer matrix.

To further exploit the discrete nature of these SERS substrates, we devised an experiment using a small number (around 75) of beads, for the ultradetection of either 1NAT or toluidine blue (TB). 1NAT is an aromatic thiol, non-resonant in the visible and NIR (Fig. 4A). Thus, upon excitation with the 830 nm laser line it would yield pure SERS, with almost no enhancement contribution due to electronic resonance. Under these conditions and by dramatically decreasing the number of nanoparticles by using the Ag–agarose beads, SERS signals of 1NAT could be fully identified down to concentrations of 10⁻¹⁰ M (Fig. 4B), two orders of magnitude lower than what has been possible using conventional colloidal silver suspensions.[18] The same experiment was then replicated using a resonant analyte. TB is a blue dye, characterized by an electronic absorption band at 625 nm that, when

Fig. 2 Optical (A) and SEM images (B and C) of the surfaces of the Ag–agarose beads. (D) Cross-sectional and high resolution SEM images of Ag particles inside the beads.

Fig. 4 (A) Electronic absorption and emission spectra for 1NAT and TB. (B) Ultrasensitive detection of 1NAT on Ag–agarose beads upon excitation with an 830 nm laser line. (C) Ultrasensitive detection of TB upon excitation with a 633 nm laser line. Molecular models for 1NAT and TB are included for reference.

excited with a red light, leads to emission at 688 nm (Fig. 4A). In this case, upon excitation with a 633 nm laser line, TB should yield surface-enhanced resonance Raman scattering (SERRS) rather than SERS. Fig. 4C shows that under these conditions, the SERRS signal from TB is fully recognized down to concentrations as low as 10^{-15} M, two orders of magnitude lower than the concentrations employed for ultradetection at the single molecule regime in proof-of-concept experiments.[4,6] This further demonstrates the efficiency of Ag–agarose beads to act as optical accumulators due to their ability to adsorb large amounts of analyte.

Conclusions

Highly SERS-active silver–agarose nanocomposite beads were fabricated within microdroplets by means of a biphasic microfluidic system. This method yields a high uniformity in size and morphology, as well as the appropriate size to allow identification of beads with a conventional optical microscope, so that the SERS analysis can be restricted to a single bead, thereby strongly reducing the amount of material needed for detection of the analyte. We can foresee straightforward applications of this new system in multiplexed ultrasensitive detection, for analysis both in the gas phase and in solution.

Experimental methods

Materials

Unless otherwise stated, all chemicals were purchased from Sigma-Aldrich. Glassware was cleaned with aqua regia and

extensively washed with water. Milli-Q water (Millipore) was used throughout all of the experiments.

Device fabrication

The microfluidic PDMS/glass device was fabricated by conventional soft lithography methods.[32] Briefly, the device was first designed with Autocad 2007 (Autodesk), and a dark-field mask was printed (Circuitgraphics). SU-8 2025 photoresist (Micro-Chem) was spin-coated onto a silicon wafer (diameter: 76.2 mm, Compart Technology Ltd.) at 500 rpm for 5 s and then ramped to 1000 rpm at an acceleration of 300 rpm s^{-1} for 33 s. This gave a final film thickness of 75 μm, as measured by profilometry on the finished master (DekTak 150). After spinning, the wafer was prebaked (3 min at 65 °C, then 9 min at 95 °C and finally 3 min at 65 °C), and then exposed to UV light through the mask on a mask aligner (MJB4, Suss Microtech). After postbaking and development, the master was hard-baked for 1 min at 170 °C. A mixture of poly(dimethylsiloxane) (PDMS, Sylgard 184) and cross-linker (ratio 10 : 1, w/w) was poured over the master, degassed and then cured overnight at 75 °C. The cured device was cut and peeled from the master, and holes for tubing were made with a biopsy punch. After treatment with air plasma for 30 s, the device was bound to a glass slide and baked at 90 °C for 30 min. The device was treated with aquapel (Pittsburg, US), a commercially available fluorosilane, for 5 min following flushing the channels with fluorous oil. The dimensions of the device are shown in Fig. 1.

Microfluidic experiments

Flows in A and B (Fig. 1) were driven with Harvard Apparatus 2000 syringe infusion pumps. Plastic syringes of 3 mL (Becton Luer-Lok Tip) and 1 mL (Braun) were used in A and B, respectively. The syringes were connected via polyethylene tubing (Intramedic, i.d. 0.38 nm) to the device. Fluorous oil (HFE-7500 3M Belgium) was used as the continuous phase, containing 0.5% w/w of EA-surfactant (Raindance Technologies), in inlet B. The dispersed phase (inlet A) was formed by a mixture of agarose 1% (Type IX-A) and AgNO$_3$ 0.5 M. The flow rate was 1000 μL h^{-1} and 5000 μL h^{-1} in A and B, respectively. The experiment was carried out at approximately 30 °C to avoid the gelation of the agarose solution. The formed droplets were collected in a plastic tube on ice to gelate the agarose once the beads were produced. The agarose beads were extracted into an aqueous phase using 1H,1H,2H,2H-perfluoro-1-octanol, 97%.

AgNPs synthesis

For the reduction of Ag$^+$ inside the agarose droplets, hydrazine (200 μL, 30 mM) was added to 200 μL of the sample. The sample changed its transparent initial colour to dark green, indicating the formation of the AgNPs inside the agarose beads. Excess of reducing agent was removed by centrifugation.

Characterization

Scanning electron microscopy (SEM) images were obtained with a JEOL JSM 6700F field-emission microscope, using either lower secondary electron image (LEI) or secondary electron image

(SEI) detector. Dark field optical images and spectra were acquired using a Zeiss Axio Observer microscope with inverted illumination. Light from a 100 W halogen bulb was directed onto the sample through a dark-field condenser with a numerical aperture of 0.8. The scattered light was collected by a 40× dry objective coupled to a spectrometer (Acton SpectraPro 2150i). The spectrum from a microdroplet was normalised by subtracting the background scattering from a clean, neighbouring region of the substrate. XPS analysis of the samples was performed with a VG Escalab 250 iXL ESCA instrument (VG Scientific), equipped with $Al_{K\alpha}$ 1.2 monochromatic radiation at 1486.92 eV, X-ray source.

Surface-enhanced Raman scattering spectroscopy

SERS experiments were conducted in a micro-Renishaw InVia Reflex system. The spectrograph uses high resolution gratings with additional band-pass filter optics, a confocal microscope and a 2D-CCD camera. Several laser excitation energies were employed, including laser lines at 532 nm (Nd:Yag), 633 nm (HeNe), 785 and 830 nm (diode). Measurements were made in a confocal microscope in backscattering geometry using 50× or 20× objectives with NA values of 0.75 and 0.40, respectively. For SERS characterization, 10 μL of a 1-naphthalenethiol (1NAT, Across Organics) 10^{-3} M solution was added to 1 mL of the sample. 10 μL of the mixture was then cast and air-dried onto a glass slide. SERS maps were collected by means of the Renishaw StreamLine accessory.

1NAT and toluidine blue (TB) solutions with concentrations ranging from 10^{-5} to 10^{-16} M were prepared. 10 μL of the sample (containing approximately 75 agarose beads) was added to 10 mL of each analyte solution. All the experiments were incubated for 24 hours. After casting one droplet of each experiment onto a glass slide, SERS was collected at random positions.

Acknowledgements

References

1 R. A. Alvarez-Puebla and L. M. Liz-Marzan, *Small*, 2010, **6**, 604–610.
2 R. A. Alvarez-Puebla and L. M. Liz-Marzan, *Energy Environ. Sci.*, 2010, **3**, 1011–1017.
3 X.-M. Qian and S. M. Nie, *Chem. Soc. Rev.*, 2008, **37**, 912–920.
4 N. P. W. Pieczonka and R. F. Aroca, *Chem. Soc. Rev.*, 2008, **37**, 946–954.
5 J. Kneipp, H. Kneipp and K. Kneipp, *Chem. Soc. Rev.*, 2008, **37**, 1052–1060.
6 R. F. Aroca, *Surface Enhanced Vibrational Spectroscopy*, Wiley, New York, 2006.
7 A. M. Michaels, M. Nirmal and L. E. Brus, *J. Am. Chem. Soc.*, 1999, **121**, 9932–9939.
8 S. K. Ghosh and T. Pal, *Chem. Rev.*, 2007, **107**, 4797–4862.
9 G. Braun, I. Pavel, A. R. Morrill, D. S. Seferos, G. C. Bazan, N. O. Reich and M. Moskovits, *J. Am. Chem. Soc.*, 2007, **129**, 7760–7761.
10 S. Bálint, M. P. Kreuzer, S. Rao, G. Badenes, P. Miskovský and D. Petrov, *J. Phys. Chem. C*, 2009, **113**, 17724–17729.
11 M. Sanles-Sobrido, L. Rodriguez-Lorenzo, S. Lorenzo-Abalde, A. Gonzalez-Fernandez, M. A. Correa-Duarte, R. A. Alvarez-Puebla and L. M. Liz-Marzan, *Nanoscale*, 2009, **1**, 153–158.
12 A. A. Farah, J. P. Bravo-Vasquez, R. A. Alvarez-Puebla, J. Y. Cho and H. Fenniri, *Small*, 2009, **5**, 1283–1286.
13 Y. Kobayashi, V. Salgueirino-Maceira and L. M. Liz-Marzan, *Chem. Mater.*, 2001, **13**, 1630–1633.
14 M. Spuch-Calvar, L. Rodriguez-Lorenzo, M. P. Morales, R. A. Alvarez-Puebla and L. M. Liz-Marzan, *J. Phys. Chem. C*, 2009, **113**, 3373–3377.
15 R. Jin, Y. C. Cao, C. S. Thaxton and C. A. Mirkin, *Small*, 2006, **2**, 375–380.
16 J.-H. Lee, M. A. Mahmoud, V. B. Sitterle, J. J. Sitterle and J. C. Meredith, *Chem. Mater.*, 2009, **21**, 5654–5663.
17 J.-H. Lee, M. A. Mahmoud, V. Sitterle, J. Sitterle and J. C. Meredith, *J. Am. Chem. Soc.*, 2009, **131**, 5048–5049.
18 S. Abalde-Cela, S. Ho, B. Rodriguez-Gonzalez, M. A. Correa-Duarte, R. A. Alvarez-Puebla, L. M. Liz-Marzan and N. A. Kotov, *Angew. Chem., Int. Ed.*, 2009, **48**, 5326–5329.
19 F. J. Garcia de Abajo, *Rev. Mod. Phys.*, 2007, **79**, 1267–1290.
20 P. Aldeanueva-Potel, E. Faoucher, R. A. Alvarez-Puebla, L. M. Liz-Marzan and M. Brust, *Anal. Chem.*, 2009, **81**, 9233–9238.
21 R. A. Alvarez-Puebla, R. Contreras-Caceres, I. Pastoriza-Santos, J. Perez-Juste and L. M. Liz-Marzan, *Angew. Chem., Int. Ed.*, 2009, **48**, 138–143.
22 R. A. Alvarez-Puebla and R. F. Aroca, *Anal. Chem.*, 2009, **81**, 2280–2285.
23 C. Jones, K. Bantz and C. Haynes, *Anal. Bioanal. Chem.*, 2009, **394**, 303–311.
24 A. D. Strickland and C. A. Batt, *Anal. Chem.*, 2009, **81**, 2895–2903.
25 L. Guerrini, J. V. Garcia-Ramos, C. Domingo and S. Sanchez-Cortes, *Anal. Chem.*, 2009, **81**, 1418–1425.
26 Y. Zhao, J. N. Newton, J. Liu and A. Wei, *Langmuir*, 2009, **25**, 13833–13839.
27 A. B. Theberge, F. Courtois, Y. Schaerli, M. Fischlechner, C. Abell, F. Hollfelder and W. T. S. Huck, *Angew. Chem., Int. Ed.*, 2010, **49**, 5846–5868.
28 R. K. Shah, J. W. Kim, J. J. Agresti, D. A. Weitz and L. Y. Chu, *Soft Matter*, 2008, **4**, 2303–2309.
29 S. Q. Xu, Z. H. Nie, M. Seo, P. Lewis, E. Kumacheva, H. A. Stone, P. Garstecki, D. B. Weibel, I. Gitlin and G. M. Whitesides, *Angew. Chem., Int. Ed.*, 2005, **44**, 724–728.
30 S. Sugiura, T. Oda, Y. Izumida, Y. Aoyagi, M. Satake, A. Ochiai, N. Ohkohchi and M. Nakajima, *Biomaterials*, 2005, **26**, 3327–3331.
31 Q. Xu, M. Hashimoto, T. T. Dang, T. Hoare, D. S. Kohane, G. M. Whitesides, R. Langer, D. G. Anderson and H. David, *Small*, 2009, **5**, 1575–1581.
32 Y. Xia and G. M. Whitesides, *Angew. Chem., Int. Ed.*, 1998, **37**, 550–575.
33 L. Rodriguez-Lorenzo, R. A. Alvarez-Puebla, I. Pastoriza-Santos, S. Mazzucco, O. Stephan, M. Kociak, L. M. Liz-Marzan and F. J. G. de Abajo, *J. Am. Chem. Soc.*, 2009, **131**, 4616–4618.
34 J. C. Love, L. A. Estroff, J. K. Kriebel, R. G. Nuzzo and G. M. Whitesides, *Chem. Rev.*, 2005, **105**, 1103–1170.
35 P. Mulvaney, *Langmuir*, 1996, **12**, 788–800.